Soft Matter

A multiscale approach to uncover the self-assembly of ligand-covered palladium nanocubes

Journal:	*Soft Matter*
Manuscript ID	SM-ART-08-2023-001140.R2
Article Type:	Paper
Date Submitted by the Author:	16-Oct-2023
Complete List of Authors:	Chen, Xiangyu; Johns Hopkins University, Chemical and Biomolecular Engineering Vo, Thi; Johns Hopkins University, Chemical and Biomolecular Engineering Clancy, Paulette; Johns Hopkins University, Chemical and Biomolecular Engr.

A multiscale approach to uncover the self-assembly of ligand-covered palladium nanocubes

Xiangyu Chen[1], Thi Vo[1], Paulette Clancy[1*]

[1]Department of Chemical and Biomolecular Engineering, Johns Hopkins University, Baltimore, MD, 21218, USA
[*] Corresponding author

1 Abstract

Ligand-mediated superlattice assemblies of metallic nanocrystals represent a new type of mesoscale materials whose structural ordering directly influence emergent collective properties. However, universal control over the spatial and orientational ordering of their constitutive components remains an open challenge. One major barrier contributing to the lack of programmability in these nanoscale building blocks revolves around a gap in fundamental understanding of how ligand-mediated interactions at the particle level propagate to macroscopic and mesoscale behaviors. Here, we employ a combination of scaling theory and coarse-grained simulations to develop a multiscale modeling framework capable of bridging across hierarchical assembly length scales for a model system of ligand-functionalized nanocubes (here, Pd). We first employ atomistic simulations to characterize how specific ligand-ligand interactions influence the local behaviors between neighboring Pd nanocubes. We then utilize a mean-field scaling theory to both rationalize the observed behaviors as well as compute a coarse-grained effective pairwise potential between nanocubes capable of reproducing atomistic behaviors at the mesoscale. Furthermore, our simulations reveal that a complex interplay between ligand-ligand interactions is directly responsible for a a shift in macroscopic ordering between neighboring nanocubes. Our results, therefore, provides a critical step forward in establishing a multiscale understanding of ligand-functionalized nanocrystalline assemblies that can be subsequently leveraged to design targeted structures exhibiting novel, emergent collective properties.

2 Introduction

Recent advances in nanoscale synthesis have revolutionalized our ability to control the self-organization of microscopic components into long-range, macroscopic structures. [1–4] In particular, metallic nanoparticles with surface-functionalized ligands have emerged as a suite of versatile building blocks that can reliably and reproducibly self-assemble into both 2D and 3D structures exhibiting a wide range of interesting optical,[5, 6] plasmonic,[7, 8] and/or magnetic[9] properties. Such diverse emergent properties, coupled with control over spatial and orientational ordering, suggest that ligand-functionalized nanoparticles can provide an ideal design space for materials

discovery spanning a wide range of technologically open challenges.

Despite these fundamental advances, however, there are still major limitations that hinder the usage of nanoscale self-assembly on an industrial scale. Firstly, directing structural organization is typically system-specific, making it challenging to decouple the effect of an individual nanoparticle size/shape, its functionalized ligands, and inter-nanoparticle interactions from the structure into which they are assembled. [10–13] Secondly, in the limit of anisotropic nanoparticle cores (*i.e.,* polyhedral nanoparticles), robust control over orientational alignment is often limited to special "lock-and-key" interactions. [14–16] Universal control over the orientational ordering of arbitrarily shaped nanoparticles remains elusive.

To address this grand challenge, a large repository of simulation studies have been performed, aimed at characterizing the role of particle shape in driving self-assembly. [1, 2, 17–20] However, these studies rely on coarse-graining strategies that create an effective shape (core + ligand shell) to attain the computational efficiency needed to capture mesoscale assemblies in molecular simulations. Such an approach prevents direct mapping between how ligand-ligand interactions influence emergent orientational ordering between ligand-functionalized nanoparticles. This knowledge gap in fundamental understanding of how ligand-mediated interactions propagate to macroscopic behaviors makes it hard to decouple the role of the ligand shell versus nanoparticle core in driving self-assembly. While there have been computational efforts developed to tackle this key question,[21–23] they are often limited in system size due to the need to simulate the entire ligand shell coating the nanoparticle core and therefore cannot predict, *a priori*, the emergent self-assembly superlattices. Conversely, thermodynamic perturbation theory based approaches have been successfully employed to design co-assemblies of ligand-functionalized anisotropic nanoparticles,[12, 13, 15] but these efforts focus on free energy-based phase predictions and do not provide an explanation regarding how ligand-ligand interactions propagate across multiple length scales. As a result, developing a multiscale modeling approach that is capable of bridging atomic-level simulation findings to mesoscale, hierarchical organizations is critical to further push the limits of computational materials designs.

Through this lens, ligand-functionalized nanocubes serve as the ideal model system. Nanocubes can be readily synthesized in bulk, with high precision and reproducibility.[24] Recent experimental work has discussed in depth how a superlattice rotation can critically influence structural transformations and nanocube assembly as well as thermodynamic contributions to this process. [25–27] Therefore, understanding how ligand-mediated interactions between nanocubes propagate to long-range structural organizations results in a convenient test bed in which predictions by theory and simulation can be rigorously validated in experiments. Furthermore, nanocube synthesis can easily incorporate more exotic metals, such as Ag, Pt, and Pd. This means that a fundamental understanding of hierarchical nanocube self-assembly can be immediately leveraged to design metallic nanocubes for use in catalytic, [28–30] biomedical, [31] fuel cell, [32] and hydrogen storage [33] applications.

In this paper, we use a combination of scaling theory and coarse-grained simulations to investigate interactions between nanocubes during the self-assembly process. To ground our studies in experimentally realizable systems, we choose dodecanethiol-functionalized palladium nanocubes as the system of interest. [34–38] We first characterize the thermodynamic and kinetic behaviors for ligand-coated Pd nanocubes using coarse-grained atomistic molecular dynamics simula-

tions as a function of both ligand length and solvent quality. Simulations reveal that the ligand length plays a significant role in controlling the free energy barriers between two competing local configurations – "face-to-face" and "brick-wall" – that ultimately influence the rotational and translational assembly pathways of the nanocube superlattices. To bridge atomistic behaviors to mesoscale assemblies, we employ our previously developed scaling theory to predict the shape of the ligand shell (corona) about a nanocube. We then utilize the predicted corona shape to compute an effective pairwise potential between ligand-functionalized nanocubes that captures the trends observed from atomistic simulations. This effective potential is then employed to perform large-scale assembly simulations, reproducing atomistic behaviors at the mesoscale. Theory as well as atomistic and coarse-grained simulations additionally reveal a cooperative, translation-rotation process that drives transition from a brick-wall to face-to-face assembly motif with decreasing ligand lengths.

The agreement between atomistic and coarse-grained simulations, coupled with a predictive theory capable of bridging behaviors across scales, suggest that our modeling framework can be used as a tool to design nanoscale building blocks. Furthermore, the observed tunability in self-assembled morphology indicates that ligand engineering can be employed as a powerful "handle" to select for different orderings in nanocube assemblies. Our results provide a critical step forward in the establishment of a multiscale understanding of ligand-functionalized nanoparticle self-assembly, where interactions between individual particles can be tuned at the molecular level to target assemblies with novel, emergent collective properties.

3 Theory and Computational Methods

3.1 Force fields and Molecular Dynamics simulation set-up

The coarse-grained models used in this paper are designed to capture relevant intra- and intermolecular interactions to represent their intrinsic behavior. We used the semi-empirical force field developed by Paul *et al.* to represent the alkyl-groups for the ligand molecules grafted onto the Pd metal core, as this model is known to avoid the tendency to form unphysical "brush"-like structures exhibited by models such as OPLS. [35, 37, 38] More details of this comparison are provided in the SI, including a list of parameters used in these models.

All the atomistic molecular dynamics (MD) simulations performed in this work were conducted using LAMMPS, a popular MD code developed by Sandia National Laboratory.[39] We used hollow nanocubes of Pd consisting of a 7x7x7 supercell which has length of 27 Å. We fixed in place the outer layer of atoms comprising the Pd cubes such that each cube then moved as a rigid body to maintain structural integrity. We defined the interactions between Pd atoms to consist only of van der Waals interactions to be consistent with the parameterization used to fit a force field for transition metals like Pd. [34] The Pd nanocubes are covered in ligands with a density of 6 ligand/nm^2, based on typical experimental values, and attached to the Pd particle by the formation of a single Pd-S bond at the Pd surface. These attachment points are randomly chosen from amongst the available surface Pd atoms and the Pd-S bond is not breakable. We defined the interaction between palladium and sulfur atoms on the ligand as a simple harmonic bond, approximated as being the same as those for platinum-sulfur interactions for which parameters already exist. [35] We used a coarse-grained "united atom" (UA) model [36, 37] to represent the ligand molecules and a TraPPE-UA coarse-grained force field to represent the toluene solvent molecules. [38] The

parameters used in this work are provided in the Supplemental Information Table S1-S7.

3.2 Free energy studies using Thermodynamic Integration and Steered Molecular Dynamics

3.2.1 Thermodynamic Integration

We used the well-established Thermodynamic Integration (TI) method [40–42] to calculate the free energy change that results when a single Pd nanocube moves laterally across the surface of a Pd surface from an initial position in a face-to-face configuration, through an intermediate brick-wall configuration, and back to a final face-to-face configuration, as illustrated in Figure 1. In the TI method, the distance travelled by the nanocube as it traverses the reaction coordinate between face-to-face and brick-wall configurations is divided into a set of "frames" (or "windows"). At each frame of the TI calculations, we fixed the positions of the Pd atoms within each nanocube so that it moved as a coherent cubic entity but allowed the ligand molecules and solvent molecules to move freely to minimize their free energy.

Initially, we ran an MD simulation in the microcanonical ensemble, NVE, for 0.5 *ns* to allow any overlapping atoms time to move out of the way of one another. Then we ran MD in the isothermal (NVT) ensemble at 298 K for at least 3 *ns* for each of windows (15 to 17 windows, depending on the length of the ligand) in the TI or until the errors in the forces were less than 0.5 kcal/mol/Å.

3.2.2 Steered Molecular Dynamics

Like TI, Steered Molecular Dynamics (SMD) also allows us to calculate the free energy associated with a reaction pathway. But each of them serves a different purpose. The TI method assumes that you know the reaction coordinate and want to establish an accurate free energy barrier to move from point A to point B (from an initial to a final position). SMD makes few, if any, assumptions of the nature of the reaction coordinate; it simply "pulls" two entities together (or "pushes" them apart) using one (or more) tethering points between the two moieties (typically, their centers of mass). But it does not prescribe the reaction coordinate that it takes during the pulling/pushing process. A key parameter here is the "pulling" velocity that determines the speed at which the entities are pulled apart. SMD has the reputation of producing less accurate free energy barriers than those from TI.

We have found it best to deploy both methods in this fashion: SMD is used to determine the reaction coordinate in a relatively unbiased fashion. Then we employ TI (adopting the SMD-determined reaction coordinate) to determine more accurate values of the free energy barriers. In this case, however, there was no need to link the two methods in this way, as we had a clear idea of the trajectories that we wanted to investigate.

3.3 Tendency for vacancies to "self-heal" in a 2D array of Pd nanocubes

The second study investigated the experimental observation that vacancies in a 2D array of Pd nanocubes would be filled ("healed") by the movement of other ligand-clad nanocubes near the vacancy. For this study, we took advantage of the periodic nature of the simulation box to create a 3 x 5 lattice of nanocubes that mimicked an infinite 2D Pd superlattice array. This simulation

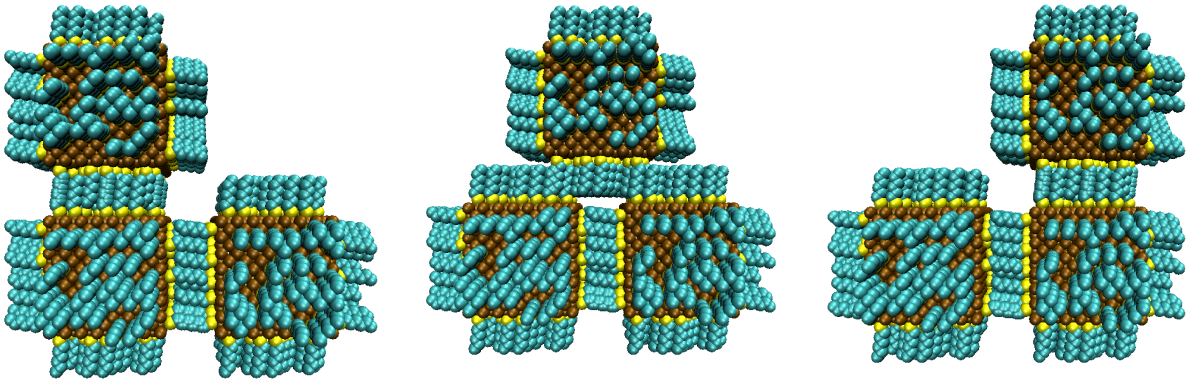

(a) face-to-face config. (b) brick-wall config. (c) back to face-to-face config.

Figure 1: Reaction pathway (L-R) used for the TI and SMD calculations to calculate the free energy change from face-to-face (a) to brick-wall (b) and back again to face-to-face (c) in a three-nanocube system. Here, we only display nanocubes with short, "C-6", ligands containing a six-carbon-atom chain. Pd atoms are shown in brown, carbon atoms in blue and sulfur atoms in yellow. Solvent molecules are not included in this figure for clarity.

fixed the positions of the center of mass (CoM) of all the nanocubes, except for two nanocubes in the center of the array (marked as A and B in Figure 2) that are separated by a vacancy in the array. Nanocubes A and B were allowed to move freely to move under the influence of the forces between them. The ligands on the surrounding ("frozen") particles were also allowed to move. A spring force was applied between connection points at the CoM of the two nanocubes to pull the mobile nanocube B towards the vacancy and ultimately to reside next to mobile nanocube A. This is the essence of a Steered Molecular Dynamics (SMD) simulation. The pulling speed of the spring was 0.25 nm/ns.

3.4 Effect of ligand length

We ran a set of TI simulations in which we varied the ligand length, studying 6-, 9-, 12- and 15- carbon-atom backbones. We refer to this later as "C-n" where n is the number of the carbon atoms, to examine how the length of the ligand affected the free energies associated with the configurational change between face-to-face (F2F) and brick-wall (BW) stacking. We adjusted the distance between each Pd nanocube based on the length of the ligand so that the unrelaxed ligand molecules were fully interdigitated, but not touching the Pd atoms.

3.5 Scaling theory for ligand shell shape prediction

To predict the shape of the ligand shell (corona) about the nanocube, we employ our previously developed scaling theory that has shown successes designing co-assemblies of nanocubes and nanotriangular prisms.[13, 15] Briefly, our theory predicts the ligand distribution about the core nanocube as a function of experimental handles such as grafting density (σ), ligand length (N), and core size (r_o). For ligand-functionalized nanocubes, the predicted end-to-end distance (R) of an end-functionalized ligand takes the form: $R \sim r_o \sigma^{1/4} b^{1/2} N^{1/2} \Omega^{-3/4} [b/r_o]^{1/2}$, where b is the Kuhn monomer size and Ω is a composite parameter defining both shape and surface position of

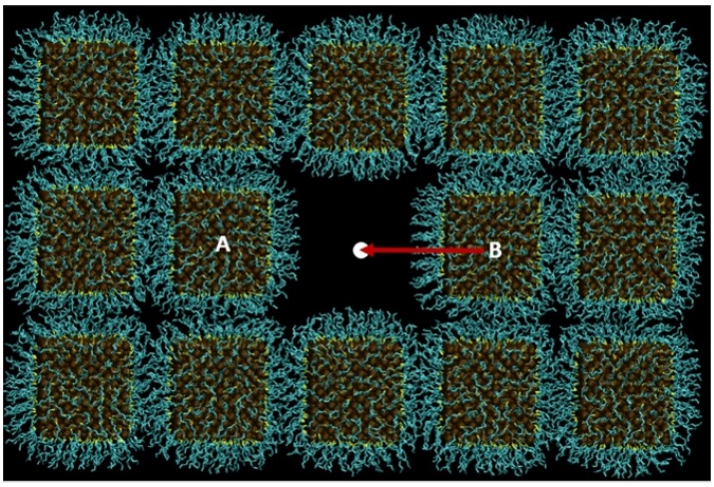

Figure 2: The initial set up of the Steered Molecular Dynamics simulation that will pull particle B towards particle A and hence "heal" the vacancy. Nanocubes in the surrounding outer layer of the lattice were fixed in place; the central two particles (A and B) can move freely. We applied a spring force to pull nanocube B towards the vacancy as illustrated by the red arrow. All the toluene solvent molecules are hidden for clarity. Pd atoms are shown in brown, C atoms in blue and S atoms in yellow. Solvent molecules are transparent in this figure. The background is painted black to better visualize the ligand molecules.

the nanoparticle core. We note that this relation is a generalization of the brush scaling theory to the limit of shorter ligand lengths, where the *n*-alkanes are too short to span into the brush's semi-dilute regime. Using the above equation for R, the Flory energy (F) can then be defined as: $\beta F \sim R^2/Nb^2 + \nu N^2 f/(\Omega R)^3$, where ν is the monomer's excluded volume. Using this free energy, we then perform Monte Carlo (MC) grafting simulations to anchor chains at different positions on the nanocube's surface using the standard Metropolis acceptance criterion, where the acceptance probability is defined as $P_{graft} \sim e^{-\beta F}$. Averaging over 1E5 MC simulations yields a thermodynamic average of the effective shape of the ligand shell about the nanocube core.

3.6 Coarse-grained mesoscale simulation of ligand-functionalized nanocubes

In order to achieve mesoscale assemblies, we first develop a coarse-grained model using the predicted corona shapes obtained from scaling theory. Our goal here is to preserve the range of interactions between ligand-functionalized nanocubes but reduce force calculations between particles into one, single effective pairwise potential. Here, we compute a potential of mean force (PMF) between two ligand-functionalized nanocubes, as a function of their center-to-center distance. PMF calculations are performed by explicitly considering all ligands on the nanocube surface and summing up all possible interactions with ligands from the neighboring nanocube. The computed PMFs are then taken to be an effective interaction potential, $V(r)$, between nanocubes for use in simulations (Fig. 5b,c). By inspection, the computed $V(r)$ have functional forms similar to that of a Lennard-Jones potential, albeit with varying ranges of interactions. This immediately suggest the use of the Mie potential for implementation within a traditional molecular dynamics engine.

As such, we fit the computed potential to different exponents of the Mie potential to capture the correct range of interaction for assembly simulations.

Since the computed $V(r)$ is isotropic, we additionally employ our generalized anisotropic potential fo rigorously simulate the nanocube core to preserve the correct particle geometry.[43] This potential is already implemented and readily available in the HOOMD-Blue simulation engine, motivating our usage of HOOMD for all mesoscale simulations.[44] All simulations are performed using an NVT integrator for 1000 nanocubes at a particle volume fraction of 0.425 (below the shape-driven crystallization transition for cubes), $kT = 1.0$, and an integration time step of $dt = 0.00025$. Equilibration and production run times are 2E6 and 1E7, respectively.

4 Results and Discussion

4.1 Stacking proclivities for Pd nanocubes

We calculated the free energy in the three-nanocube system using TI, which allowed us to include the rather significant entropic contributions to the stacking behavior between two different configurations of Pd nanocubes, face-to-face and brick-wall. We used Thermodynamic Integration (TI) and Steered Molecular Dynamics for this purpose.

The free energy landscape obtained from TI calculations of nanocubes in vacuum is shown in Figure 3. As is typical in vacuum simulations, when the Pd nanocube was slid across the nanocubes below it (from Figure 1a to Figure 1b), it experienced a large free energy barrier, regardless of ligand length, as we shall show in the next section. The maximum free energy occurs when the system is in the brick-wall configuration. As the top Pd nanocube returns to a F2F configuration (from Figure 1b to Figure 1c), the free energy returned essentially to its initial, near-zero, free energy value. This change in free energy suggests that, for each system we studied, a F2F configuration is more thermodynamically favorable than the BW one. This confirms the experimental results of Quan *et al.* for Pt nanocubes.

4.2 Effect of ligand length

Ligand length has a pronounced effect on the free energy barrier. Figure 3 shows that the energy barrier between F2F and brick-wall configurations for short C-6 ligands in vacuum is extremely high (1356 kcal/mol). Such high energy barriers are not uncommon for systems in vacuum. The actual values are less important here than the trend as we vary ligand length. The barrier drops non-linearly and dramatically to 387, 329 and 209 kcal/mol as the ligand length increases to C-9, C-12 and C-15, respectively. As the ligand length increases, the nanocubes, of necessity, move further away from each other. The distance between nanocubes covered in C-6 ligands is 15 Å, but the distance between C-15-covered nanocubes is 24 Å. This 9 Å change in inter-nanocube distance alters the forces significantly.

We performed the TI simulations both in vacuum and in a toluene solvent to examine if, and to what extent, the presence of solvent molecules affected the stacking preference. Replacing the vacuum by including solvent molecules, here, using a TraPPE model for the toluene solvent, we found that changing the ligand lengths (from C-6 to C-9 to C-12) produced similar trends in the free energy landscape to those found in vacuum in that the free energy decreased with increasing ligand length. Longer ligands are better able to stabilize the stacking of Pd nanocubes and hence lower the free

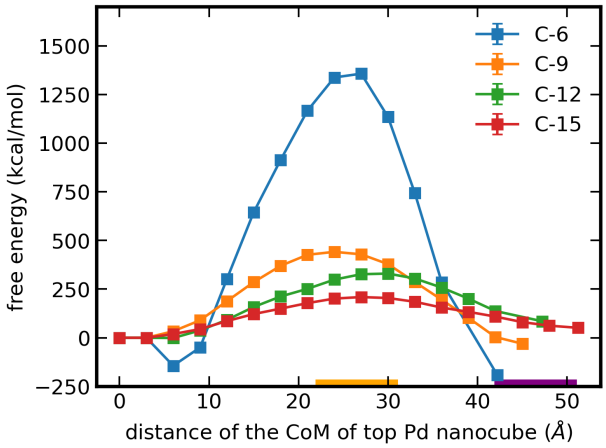

Figure 3: TI-derived free energy as a function of the location of the top nanocube in vacuum as illustrated in Figure 1. At 0 Å, the system is in the original face-to-face configuration shown in Figure 1a and the free energy is set to zero for each system. By 22-31 Å, depending on ligand length, the system has moved to the brick-wall configuration shown in Figure 1b. As the top nanocube resumes its move towards the face-to-face configuration, as shown in Figure 1c, the energy falls until it returns to the same energy value as its initial condition at 0 Å distance. The orange bar on the *x*-axis indicates the location of the brick-wall configuration at 22-31 Å, as the ligand length increases from C-6 to C-15. The purple bar indicates the location of the face-to-face configurations at 42-51Å, again depending on ligand length.

energy barriers. A comparison between results in vacuum and in toluene are plotted in Figure S2 and values of peak heights are given in Table S8. It is instructive to look at the *changes* in the maximum barrier height of free energy in the presence of toluene as you change the ligand length. For shorter C-6 and C-9 ligand lengths, the change in barrier is the largest in C-6 (a change of 284 kcal/mol), compared to C-9 (a change of 48 kcal/mol). On the other hand, for C-12, the peak in free energy is smaller in toluene compared to vacuum (a change of -75 kcal/mol). This interesting result indicates that in a solvent of coarse-grained toluene molecules, the nanocubes in brick-wall configuration are *destabilized* when covered with short ligands, but *stabilized* by longer ligands. This trend is consistent with simulation results for ligand-covered lead chalcogenide truncated nanocubes where the presence of solvent makes an FCC superlattice the preferred stacking, with a diminishing effect for longer ligand lengths. [35] Again, this reinforces the suggestion that the lack of solvent is at least partially responsible for the large free energy barriers in vacuum.

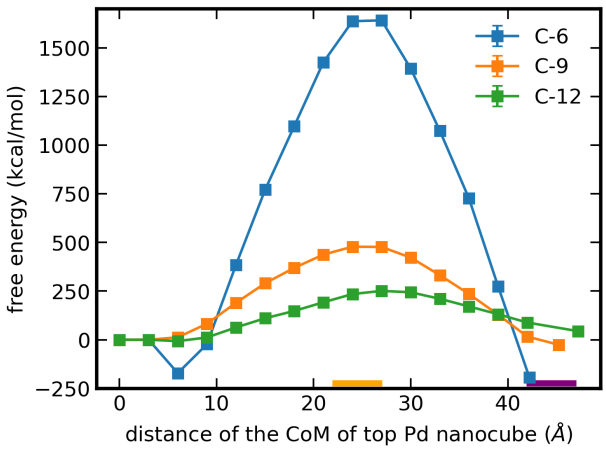

Figure 4: Effect of ligand length on TI-measured free energies in a toluene solvent. The energy barrier for movement across the surface of a nanocube decreases with ligand length. As for the vacuum results, the maximum in the free energy barrier occurs at the brick-wall configuration. The orange bar on the *x*-axis indicates the location of the brick-wall configuration at 22-27 Å, depending on the ligand length for C-6 to C-15. The purple bar indicates analogous locations of the face-to-face configurations at 42-47 Å, again depending on ligand length.

To determine the trajectory along a more unbiased reaction coordinate, we also ran a Steered Molecular Dynamics (SMD) simulation of the three-nanocube configuration shown in Figure 1 with a pulling speed of 0.25 nm/ns, watching the trajectory as the upper nanocube moved across the two lower ones. We used C-9 ligands for the SMD run as this maintained roughly the same ratio of ligand length-to-cube diameter as in the experiments. It was also computationally more tractable than using longer ligands. SMD simulations allowed us to probe the origin of the large energy barriers.

In SMD simulations of the three-nanocube system in vacuum, see Figure 1, we observed a small "hop" in the horizontal direction when sliding the top nanocube moved towards the brick-wall configuration. This trajectory change in the SMD correlated well with the time point at which the system experiences a large energy barrier (1200 kcal/mol; shown in Figure S3(a)) associated with transitioning to the brick-wall configuration. There is a strong similarity between the free energy landscapes in Figure S3(a) predicted by SMD [Left] and TI [Right], since the distance in SMD is a linear function of simulation time. Both exhibit a significant energy barrier, though -as is typical- the SMD barrier height is far higher in value. Figure S3(b) [Left] shows that moving the top nanocube across the surface caused it to rotate relative to the nanocubes below it in response to the force field it experienced as it approached the brick-wall configuration. It reached a maximum rotation of 11-12° by about 10 *ns* and remained rotated by about 10-11° thereafter. Figure S3(b) [Right] shows that the rotation is uncorrelated with the free energy profile during the configurational change. Previous work has shown that similar positional entropy affects structural transformations in superlattices of face-centered cubic (fcc), body-centered cubic (bcc) and simple cubic (sc) configurations across different metal and metal oxide nanocube systems. [25, 26] We provide a visualization of the "hopping" and rotational change of the top nanocube in

Figure S4.

To explain the observed trends from a theoretical perspective, we first characterize the predicted corona shapes obtained from scaling theory and MC grafting simulations. Analysis of our results reveal two distint corona shapes - conformal and convex – that emerge as a function of varying ligand length (Figure 5a). Conformal shapes define coronas whose shape is analogous to the intrinsic geometry of the nanocube core. These coronas occur in the limit of short ligands, where ligands experience a uniform degree of confinement from their neighbors and thus organize into a uniform brush on the nanocube surface. This regime is analogous to the classical Alexander-de Gennes brushes from planar grafting.[45] As the ligand lengths increase, the chain feels a continuously greater degree of confinement from their neighbors due to the presence of more monomers within the same solid angle volume occupied by the ligand. This means that ligands will switch to more extended configurations to maximize their local free volume and reduce steric repulsions with their neighbors. Center face locations on the nanocube surface experience higher confinement due to a smaller volume available given the same solid angle. As a result, centered face ligands experience increased extension relative to their counterparts at locations nearer to corners/edges. The augmented extension at the faces shifts the planar morphology to that of a spherical cap, which we define as the convex corona.

Given that the conformal corona define short, uniform brushes about the nanocube surface, the net inter-nanocube ligand-ligand interaction is stronger for conformal coronas. This is because the total area of interaction for conformal corona is the entire face of each nanocube due to the flat geometry of the ligand shell. As such, transition via sliding (Figure 3) from face-to-face to brick-wall has to break all ligand-ligand interactions across the entire nanocube's face, giving rise to a large free energy barrier. Conversely, the convex corona has a spherical cap-like motif at center face locations. This extends the spacing between neighboring cubes, causing ligands nearer to corners and edges that are not as extended as centered face ligands to fall out of interaction range with each other. In other words, the net number of ligand-ligand interactions between neighboring faces decreases upon transition from a conformal to convex coronas, producing a decrease in the free energy barrier of the face-to-face to brick-wall transition. To quantitatively analyze the effect of corona shape in governing interparticle interactions, we compute an orientationally averaged potential of mean force (PMF) between nanocubes. Briefly, we first place ligands at nanocube surface locations predicted from scaling theory. We then assign an isotropic Lennard-Jones (LJ) interaction potential between all monomers making up the functionalized ligands. The LJ potential is employed to capture both the isotropic aggregation between monomers while simultaneously accounting for steric repulsion between neighboring ligands. We then sum over all ligand-ligand interactions, given a relative orientation, as a function of the center-to-center distance between nanocubes. This process is repeated for all relative orientations between nanocubes and then Boltzmann averaged to yield a pairwise PMF between nanocubes. The resulting PMFs confirm the trends, revealing a deep, short-range attraction for conformal coronas and a shallow, long-range attraction for convex coronas (Figure 5b).

4.3 Mechanism of nanocube reorganization as a self-healing process

We built a 2D superlattice of Pd nanocubes in a 3 x 5 array. Each nanocube was covered with C-9 ligands, consistent with our preceding smaller 3-cube SMD simulations. This array included a centrally located vacancy. We observed a similar rotation of the moving nanocube as discussed

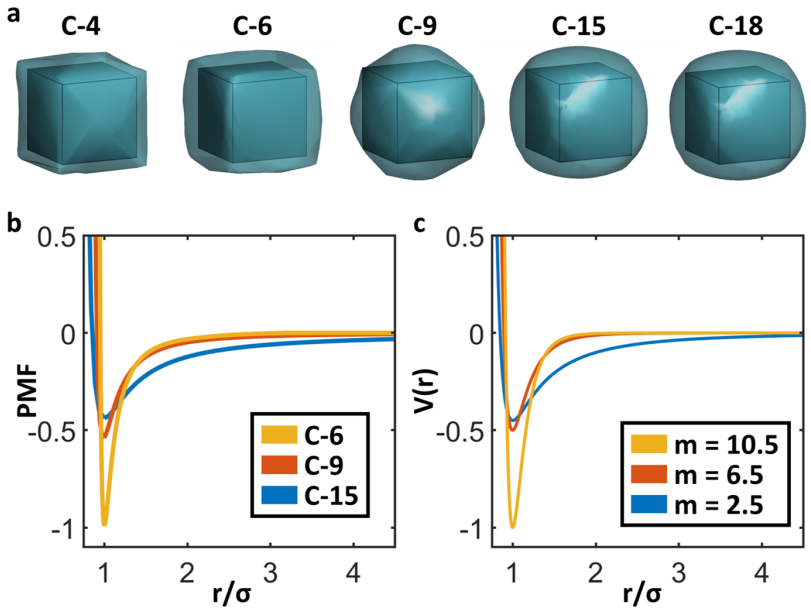

Figure 5: Theory prediction of ligand length effects. a) Visualized shape of the ligand shell (corona) as a function of alkane chain length. b) Computed PMF between two interacting ligand-functionalized nanocubes. c) Fits to PMFs from b) using the Mie potential: $V(r) = C\varepsilon\left[(\sigma/r)^n - (\sigma/r)^m\right]$, with $C = [n/(n-m)]\,(n/m)^{m/(n-m)}$ and n = 12. PMFs in b) and c) are unitless as they are scaled to the maximum well depth.

above, and shown in the snapshot in Figure S5. Nanocube B underwent a rotation as we pulled it towards the vacancy and in the direction of nanocube A, as marked in Figure 2. The space available for nanocube B to rotate was limited due to the fixed nature of the Pd atoms in the outside layer of the superlattice. The SMD simulation shows that nanocube B reached the vacancy (marked as the white dot in Figure 2) and, since the spring force was applied continuously, nanocube B kept moving towards nanocube A until it filled the original vacancy, resulting in vacancy diffusion. Analogous behaviors have been also observed in systems of hard, non-interaction nanocubes.[46] We noticed that nanocube A initially started to move towards the vacancy, but nanocube B eventually pushed it back to its original position. The net result is a disruption of a perfect face-to-face alignment in favor of a dynamic, reorganizable brick-wall-like motif. We have plotted the corresponding degree of rotation and free energy change during the simulation, and the relationship between the rotation and free energy in Figure S6(a-d).

These results indicate that a cooperative translation-rotational process, coupled with a reduction in free energy barrier, can shift the mesoscale assembly behaviors for ligand-functionalized nanocubes. To study propagation of this process to the mesoscale assembly level, we perform coarse-grained molecular dynamics simulations using a combination of the computed PMF and a generalized shaped potential[43] using the HOOMD-Blue simulation engine. To define a computationally efficient potential, we fit the computed PMFs (Figure 5b) to a Mie potential of the form: $V(r) = C\varepsilon\left[(\sigma/r)^n - (\sigma/r)^m\right]$, where $C = [n/(n-m)]\,(n/m)^{m/(n-m)}$, n is always equal to 12, and m varies to tune the width of the potential (Figure 5c). Note that increasing m tightens the interactions

range and is equivalent to decreasing ligand length.

We first performed 2D simulations of nanosquares to mimic the single layer study shown in Figure 2. We then measure the distribution of nanosquares rotation angle, averaged over the entire production run of the simulations (Figure 6a). Rapid clustering and statistical averages across the large set of simulation data are facilitated by the *freud* analysis package.[47] Results from 2D simulations reveal a broadening in the angle distribution ($P(\theta)$) with increasing ligand lengths (decreasing m). This means that nanocubes with longer ligands are able to rotate more freely (due to the decrease in energy barrier), in good agreement with the reduction in the computed free energy barrier obtained from atomistic simulations (Figure 3). We then confirm the shift from brick-wall to face-to-face lattice arrangement by computing the radial distribution function ($g(r)$) of the self-assembled lattices for different ligand lengths (Figure 6b). To extend to bulk, 3D systems, we additionally run simulations of nanocubes. Measurements of the angle distribution and radial distribution function reveal an identical $P(\theta)$ broadening and a shift from brick-wall to face-to-face alignments, respectively (Figure 6c,d). Visualization of both brick-wall and face-to-face configurations from 2D nanosquares and 3D nanocubes simulations are shown in Figure 6e-h.

To complement the $g(r)$ and snapshots in Fig. 6, we additionally compute the average Steinhardt order parameter ($\langle q_l \rangle$) for both 2D and 3D assemblies. We set $l = 4$ ($\langle q_4 \rangle$) and $l = 6$ ($\langle q_6 \rangle$) for 2D and 3D systems, respectively (Fig. 7). For 2D systems, the perfect values of $\langle q_4 \rangle$ are 0.525 ($\langle q_4 \rangle_{p,BW}$) for brick-wall and 0.825 ($\langle q_4 \rangle_{p,FF}$) for face-to-face configurations. For 3D systems, the perfect values of $\langle q_6 \rangle$ is 0.476 ($\langle q_6 \rangle_{p,BW}$) for brick-wall and 0.363 ($\langle q_6 \rangle_{p,FF}$) for face-to-face configurations. These values are plotted as solid horizontal lines in Fig. 7. By inspection, Fig. 7 corroborates the transition observed from Fig. 6, where increasing m drives a transition from the brick-wall to face-to-face configuration. Lastly, to show that particle mobility and vacancy diffusion drive the brick-wall to face-to-face transition, we compute the average fraction of particles with a rotated angle greater than 12° across the production run for both 2D and 3D systems (Figure 8). Results from Figure 8 reveal an exponential decay in the fraction of rotated particles with decreasing ligand lengths (decreasing m), confirming both the sharp drop-off in free energy barrier from atomistic simulations, as well as a proposed mechanism of vacancy diffusion-driven lattice reorganization.

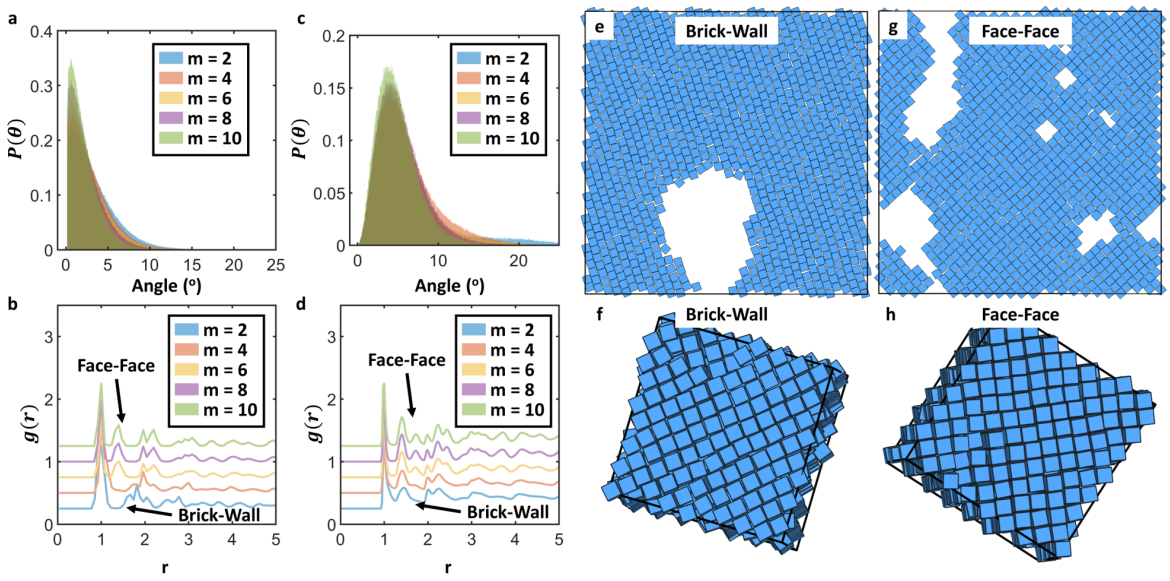

Figure 6: Coarse-grained mesoscale simulations of nanocube self-assembly. Angle distribution ($P(\theta)$) for a) 2D nanosquares and c) 3D nanocubes as a function of increasing Mie exponent m (decreasing ligand length). Radial distribution function ($g(r)$) for b) 2D nanosquares and d) 3D nanocubes as a function of increasing m reveal a transition from brick-wall to face-to-face configurations. Values of $g(r)$ are offset in y for visualization purposes. Simulation snapshots for 2D nanosquares in e) brick-wall and f) face-to-face configurations and 3D nanocubes in f) brick-wall and h) face-to-face configurations.

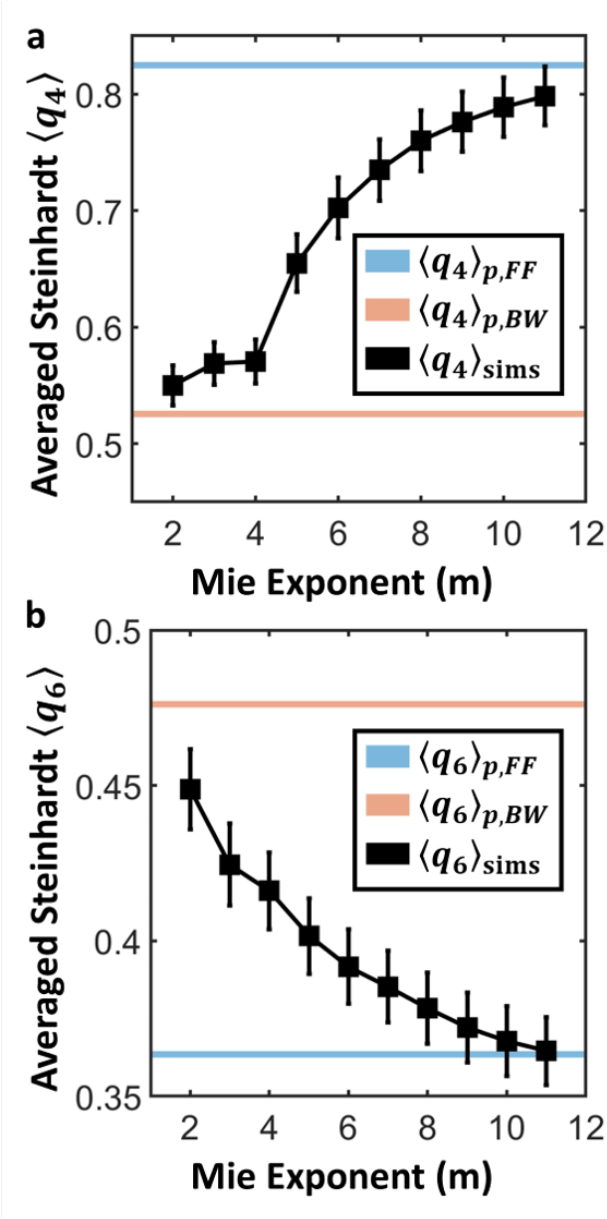

Figure 7: Comparison of average Steinhardt order parameter as a function of Mie exponent m for a) 2D nanosquares ($\langle q_4 \rangle$) and b) 3D nanocubes ($\langle q_6 \rangle$). Horizontal lines indicate the perfect values of the face-face (FF) and brick-wall (BW) configurations. We observe a quantitative transition from the brick-wall to face-face assembly motif with increase Mie exponent m.

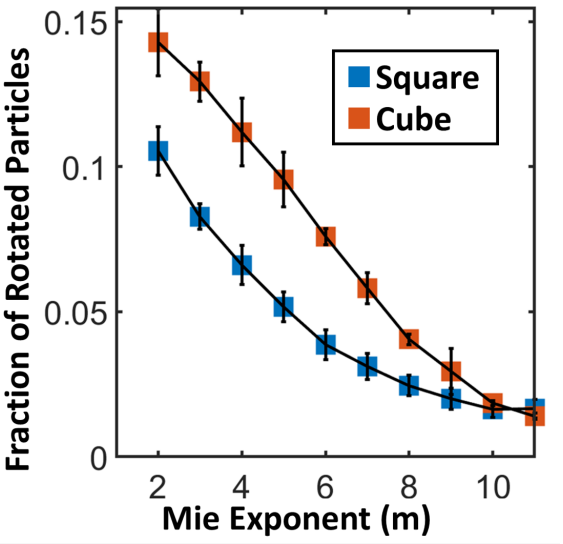

Figure 8: Measured fraction of particles with rotational angles greater than 12° for 2D nanosquares and 3D nanocubes.

5 Conclusions

In summary, we report a multiscale modeling approach that captures assembly behaviors for ligand-functionalized nanocubes. We employ both thermodynamic integration and steered molecular dynamics at the atomistic level to calculate the free energy of the interacting nanocubes, showing differences in stability between face-to-face and brick-wall nanocube configurations as a function of different ligand lengths and solvents. We additionally reveal a unique translation-rotation process by which nanocubes diffuse into vacancies that arise during the assembly process, where nanocubes rotate by about 10-12° as it enters the interstitial space between two face-face-aligned nanocubes. We then utilize brush scaling theory to explain the changes in both nanocube configuration and free energy barriers, directly connecting observed behaviors to ligand-ligand interactions and the emergent ligand brush morphologies for ligand-functionalized nanocubes. Lastly, we employ our theory to develop a coarse-grained simulation model that is capable of reproducing the trends reported in atomistic simulations at the mesoscale. Our work provides both a fundamental understanding of ligand-functionalized nanocubes interactions across hierarchical length scales as well as a modeling framework that can be readily extended to other nanocube core geometries to aid in the design of novel materials.

Acknowledgements

X.C. and P.C. thank the JHU Institute for Data-Intensive Engineering and Science (IDIES) and the JHU Space Program for funding this project. We thank the Advanced Research Computing at Hopkins (ARCH) core facility (rockfish.jhu.edu) for the provision of computational resources for this study. ARCH is supported by the National Science Foundation (NSF) grant number OAC 1920103.

Author contributions

X.C., T.V. and P.C. were engaged in the design of the project. X.C. and T.V. conducted the computations and analysis. X.C. P.C. and T.V. wrote the manuscript collaboratively. P.C. supervised and provided critical feedback to the project.

Competing interests

Authors declare no conflicts of interests

Materials and Correspondence

Correspondence should be addressed to Paulette Clancy at pclancy3@jhu.edu and materials request should be addressed to Xiangyu Chen at xchen150@jhu.edu

References

(1) Boles, M. A.; Engel, M.; Talapin, D. V. Self-Assembly of Colloidal Nanocrystals: From Intricate Structures to Functional Materials. *Chemical Reviews* **2016**, *116*, 11220–11289.

(2) Kahn, J. S.; Gang, O. Designer Nanomaterials through Programmable Assembly. *Angewandte Chemie International Edition* **2022**, *61*, e202105678.

(3) Talapin, D. V.; Engel, M.; Braun, P. V. Functional materials and devices by self-assembly. *MRS Bulletin* **2020**, *45*, 799–806.

(4) Rogers, W.; Shih, W.; Manoharan, V. Using DNA to program the self-assembly of colloidal nanoparticles and microparticles. *Nature Review Materials* **2016**, *1*, 16008.

(5) Wang, J.; Le-The, H.; Karamanos, T.; Suryadharma, R. N.; van den Berg, A.; Pinkse, P. W. H.; Rockstuhl, C.; Shui, L.; Eijkel, J. C. T.; Segerink, L. I. Plasmonic Nanocrystal Arrays on Photonic Crystals with Tailored Optical Resonances. *ACS Applied Materials & Interfaces* **2020**, *12*, 37657–37669.

(6) Sun, L.; Lin, H.; Kohlstedt, K. L.; Schatz, G. C.; Mirkin, C. A. Design principles for photonic crystals based on plasmonic nanoparticle superlattices. *Proceedings of the National Academy of Sciences* **2018**, *115*, 7242–7247.

(7) Duan, H.; Yang, Y.; Zhang, Y.; Yi, C.; Nie, Z.; He, J. What is next in polymer-grafted plasmonic nanoparticles? *Giant* **2020**, *4*, 100033.

(8) Mulvihill, M. J.; Ling, X. Y.; Henzie, J.; Yang, P. Anisotropic Etching of Silver Nanoparticles for Plasmonic Structures Capable of Single-Particle SERS. *Journal of the American Chemical Society* **2010**, *132*, 268–274.

(9) Liu, F.; Li, Y.; Huang, Y.; Tsyrenova, A.; Miller, K.; Zhou, L.; Qin, H.; Jiang, S. Activation and Assembly of Plasmonic-Magnetic Nanosurfactants for Encapsulation and Triggered Release. *Nano Letters* **2020**, *20*, 8773–8780.

(10) Bhargava, R. N.; Gallagher, D.; Hong, X.; Nurmikko, A. OptHeinzical properties of manganese-doped nanocrystals of ZnS. *Phys. Rev. Lett.* **1994**, *72*, 416–419.

(11) Laramy, C. R.; Lopez-Rios, H.; O'Brien, M. N.; Girard, M.; Stawicki, R. J.; Lee, B.; de la Cruz, M. O.; Mirkin, C. A. Controlled Symmetry Breaking in Colloidal Crystal Engineering with DNA. *ACS Nano* **2019**, *13*, 1412–1420.

(12) Elbert, K. C.; Vo, T.; Krook, N. M.; Zygmunt, W.; Park, J.; Yager, K. G.; Composto, R. J.; Glotzer, S. C.; Murray, C. B. Dendrimer Ligand Directed Nanoplate Assembly. *ACS Nano* **2019**, *13*, 14241–14251.

(13) Elbert, K. C.; Zygmunt, W.; Vo, T.; Vara, C. M.; Rosen, D. J.; Krook, N. M.; Glotzer, S. C.; Murray, C. B. Anisotropic nanocrystal shape and ligand design for co-assembly. *Science Advances* **2021**, *7*, eabf9402.

(14) O'Brien, M. N.; Jones, M. R.; Lee, B.; Mirkin, C. A. Anisotropic nanoparticle complementarity in DNA-mediated co-crystallization. *Nature Materials* **2015**, *14*, 833–839.

(15) Lu, F.; Vo, T.; Zhang, Y.; Frenkel, A.; Yager, K. G.; Kumar, S.; Gang, O. Unusual packing of soft-shelled nanocubes. *Science Advances* **2019**, *5*, eaaw2399.

(16) O'Brien, M. N.; Girard, M.; Lin, H.-X.; Millan, J. A.; de la Cruz, M. O.; Lee, B.; Mirkin, C. A. Exploring the zone of anisotropy and broken symmetries in DNA-mediated nanoparticle crystallization. *Proceedings of the National Academy of Sciences* **2016**, *113*, 10485–10490.

(17) Damasceno, P. F.; Engel, M.; Glotzer, S. C. Predictive Self-Assembly of Polyhedra into Complex Structures. *Science* **2012**, *337*, 453–457.
(18) Gantapara, A. P.; de Graaf, J.; van Roij, R.; Dijkstra, M. Phase Diagram and Structural Diversity of a Family of Truncated Cubes: Degenerate Close-Packed Structures and Vacancy-Rich States. *Phys. Rev. Lett.* **2013**, *111*, 015501.
(19) Agarwal, U.; Escobedo, F. A. Mesophase behaviour of polyhedral particles. *Nature Materials* **2011**, *10*, 230–235.
(20) Jones, M. R.; Seeman, N. C.; Mirkin, C. A. Programmable materials and the nature of the DNA bond. *Science* **2015**, *347*, 1260901.
(21) Travesset, A. Soft Skyrmions, Spontaneous Valence and Selection Rules in Nanoparticle Superlattices. *ACS Nano* **2017**, *11*, 5375–5382.
(22) Hallstrom, J.; Cherniukh, I.; Zha, X.; Kovalenko, M. V.; Travesset, A. Ligand Effects in Assembly of Cubic and Spherical Nanocrystals: Applications to Packing of Perovskite Nanocubes. *ACS Nano* **2023**, *17*, 7219–7228.
(23) Lee, B. H.-j.; Arya, G. Assembly mechanism of surface-functionalized nanocubes. *Nanoscale* **2022**, *14*, 3917–3928.
(24) Zhang, H.; Jin, M.; Xiong, Y.; Lim, B.; Xia, Y. Shape-Controlled Synthesis of Pd Nanocrystals and Their Catalytic Applications. *Accounts of Chemical Research* **2012**, *46*, 1783–1794.
(25) Li, R.; Bian, K.; Wang, Y.; Xu, H.; Hollingsworth, J. A.; Hanrath, T.; Fang, J.; Wang, Z. An Obtuse Rhombohedral Superlattice Assembled by Pt Nanocubes. *Nano Letters* **2015**, *15*, 6254–6260.
(26) Huang, X.; Zhu, J.; Ge, B.; Deng, K.; Wu, X.; Xiao, T.; Jiang, T.; Quan, Z.; Cao, Y. C.; Wang, Z. Understanding Fe3O4 Nanocube Assembly with Reconstruction of a Consistent Superlattice Phase Diagram. *Journal of the American Chemical Society* **2019**, *141*, 3198–3206.
(27) Huang, X.; Suit, E.; Zhu, J.; Ge, B.; Gerdes, F.; Klinke, C.; Wang, Z. Diffusion-Mediated Nucleation and Growth of fcc and bcc Nanocrystal Superlattices with Designable Assembly of Freestanding 3D Supercrystals. *Journal of the American Chemical Society* **2023**, *145*, 4500–4507.
(28) Ma, X.; Hahn, K.; Sanchez, S. Catalytic Mesoporous Janus Nanomotors for Active Cargo Delivery. *Journal of the American Chemical Society* **2015**, *137*, 4976–4979.
(29) Wu, Z.; Li, L.; Liao, T.; Chen, X.; Jiang, W.; Luo, W.; Yang, J.; Sun, Z. Janus nanoarchitectures: From structural design to catalytic applications. *Nano Today* **2018**, *22*, 62–82.
(30) *Palladium Emissions in the Environment*; Zereini, F., Alt, F., Eds.; Springer Berlin Heidelberg: 2006.
(31) Phan, T. T. V.; Hoang, G.; Nguyen, V. T.; Nguyen, T. P.; Kim, H. H.; Mondal, S.; Manivasagan, P.; Moorthy, M. S.; Lee, K. D.; Junghwan, O. Chitosan as a stabilizer and size-control agent for synthesis of porous flower-shaped palladium nanoparticles and their applications on photo-based therapies. *Carbohydrate Polymers* **2019**, *205*, 340–352.
(32) Miyaura, N.; Yamada, K.; Suzuki, A. A new stereospecific cross-coupling by the palladium-catalyzed reaction of 1-alkenylboranes with 1-alkenyl or 1-alkynyl halides. *Tetrahedron Letters* **1979**, *20*, 3437–3440.
(33) Adams, B. D.; Chen, A. The role of palladium in a hydrogen economy. *Materials Today* **2011**, *14*, 282–289.

(34) Heinz, H.; Vaia, R.; Farmer, B.; Naik, R. Accurate simulation of surfaces and interfaces of face-centered cubic metals using 12- 6 and 9- 6 Lennard-Jones potentials. *The Journal of Physical Chemistry C* **2008**, *112*, 17281–17290.
(35) Kaushik, A. P.; Clancy, P. Solvent-driven symmetry of self-assembled nanocrystal superlattices—A computational study. *Journal of computational chemistry* **2013**, *34*, 523–532.
(36) Sebesta, F.; Slama, V.; Melcr, J.; Futera, Z.; Burda, J. V. Estimation of transition-metal empirical parameters for molecular mechanical force fields. *Journal of Chemical Theory and Computation* **2016**, *12*, 3681–3688.
(37) Paul, W.; Yoon, D. Y.; Smith, G. D. An optimized united atom model for simulations of polymethylene melts. *The Journal of chemical physics* **1995**, *103*, 1702–1709.
(38) Liu, X.; Ni, Y; He, L. Molecular dynamics simulation of interparticle spacing and many-body effect in gold supracrystals. *Nanotechnology* **2016**, *27*, 135707.
(39) Thompson, A. P.; Aktulga, H. M.; Berger, R.; Bolintineanu, D. S.; Brown, W. M.; Crozier, P. S.; int Veld, P. J.; Kohlmeyer, A.; Moore, S. G.; Nguyen, T. D.; Shan, R.; Stevens, M. J.; Tranchida, J.; Trott, C.; Plimpton, S. J. LAMMPS - a flexible simulation tool for particle-based materials modeling at the atomic, meso, and continuum scales. *Computer Physics Communications* **2022**, *271*, 108171.
(40) Frenkel, D.; Smit, B., *Understanding molecular simulation: from algorithms to applications*; Academic Press: 2002.
(41) Kirkwood, J. G. Statistical Mechanics of Fluid Mixtures. *The Journal of Chemical Physics* **1935**, *3*, 300–313.
(42) Jarzynski, C. Nonequilibrium Equality for Free Energy Differences. *Phys. Rev. Lett.* **1997**, *78*, 2690–2693.
(43) Ramasubramani, V.; Vo, T.; Anderson, J. A.; Glotzer, S. C. A mean-field approach to simulating anisotropic particles. *The Journal of Chemical Physics* **2020**, *153*, 084106.
(44) HOOMD-blue: A Python package for high-performance molecular dynamics and hard particle Monte Carlo simulations. *Computational Materials Science* **2020**, *173*, 109363.
(45) Chen, W.-L.; Cordero, R.; Tran, H.; Ober, C. K. 50th Anniversary Perspective: Polymer Brushes: Novel Surfaces for Future Materials. *Macromolecules* **2017**, *50*, 4089–4113.
(46) Smallenburg, F.; Filion, L.; Marechal, M.; Dijkstra, M. Vacancy-stabilized crystalline order in hard cubes. *Proceedings of the National Academy of Sciences* **2012**, *109*, 17886–17890.
(47) Ramasubramani, V.; Dice, B. D.; Harper, E. S.; Spellings, M. P.; Anderson, J. A.; Glotzer, S. C. freud: A software suite for high throughput analysis of particle simulation data. *Computer Physics Communications* **2020**, *254*, 107275.